NASA Grant NAG-1-1208
Frequency and Time domain Modeling of Acoustic Liner Boundary Conditions
PI: Donald B. Bliss, Duke University

Summary of Research

Introduction:

As part of a research program directed at the acoustics of advanced subsonic propulsion systems undertaken at NASA Langley, Duke University was funded to develop a boundary condition model for bulk-reacting nacelle liners. The overall objective of the Langley program was to understand and predict noise from advanced subsonic transport engines and to develop related noise control technology. The overall technical areas included: fan and propeller source noise, acoustics of ducts and duct liners, interior noise, subjective acoustics, and systems noise prediction. The Duke effort was directed toward duct liner acoustics for the development of analytical methods to characterize liner behavior in both frequency domain and time domain. A review of duct acoustics and liner technology can be found in Reference [1].

At that time, NASA Langley was investigating the propulsion concept of an advanced ducted fan, with a large diameter housed inside a relatively short duct. Fan diameters in excess of ten feet were proposed. The lengths of both the inlet and exhaust portions of the duct were to be short, probably less than half the fan diameter. The nacelle itself would be relatively thin-walled for reasons of aerodynamic efficiency. The blade-passage frequency was expected to be less than 1 kHz, and very likely in the 200 to 300 Hz range. Because of the design constraints of a short duct, a thin nacelle, and long acoustic wavelengths, the application of effective liner technology would be especially challenging.

One of the needs of the NASA Langley program was the capability to accurately and efficiently predict the behavior of the acoustic liner. The traditional point impedance method was not an adequate model for proposed liner designs. The method was too restrictive to represent bulk reacting liners and to allow for the characterization of many possible innovative liner concepts.

In the research effort at Duke, an alternative method, initially developed to handle bulk reacting layers as described in Reference [2], was extended to apply to a broad range of liner types. This method included the effect of local gradients along the liner surface, and was particularly appropriate for situations with flow over the liner and grazing incidence acoustic fields. In order to utilize time domain computational methods to solve for the propfan acoustic field, corresponding liner boundary conditions were developed for time domain solutions rather than frequency domain solutions.

Liner Modeling:

The traditional way to model acoustic liners assumes the surface is point-reacting and can be represented by a frequency dependent normal incidence impedance. This characterization is not only functionally simple, but has the significant advantage that the normal incidence impedance can be measured directly, thereby circumventing the need to calculate liner properties in a more fundamental manner. However, not all liners behave as point reacting, particularly in the presence of a grazing sound field.

Some of the liner concepts envisioned as a result of the Langley program were expected to allow communication through the liner structure. A simple example of this behavior is provided by a bulk-reacting liner constructed of absorptive porous material. To represent this liner analytically requires that the appropriate equation for wave propagation in the liner itself be solved, and conditions on velocity and pressure continuity be satisfied at the interface between the liner and the exterior acoustic field. This approach requires that the governing equation for the porous (and perhaps elastic) liner material be known, along with the various parameters that characterize the liner material, such as porosity, flow resistance, sound speed, etc. (some of which are frequency dependent). In cases where the liner construction is more complex, for instance a layered structure, modeling the liner would be even more difficult.

For simple porous media liners, References [2] and [3] have demonstrated that a boundary condition representation is still appropriate under certain conditions, thereby avoiding the need for a full solution of the wave motion within the liner. The conditions for applicability of the boundary condition approach require that the wavelength be larger than the liner thickness, and/or that there be a reasonable degree of internal dissipation to restrict the region of influence between points on the liner surface. These conditions were expected to be satisfied in the advanced ducted fan application, which represented a thin highly absorptive liner.

Porous Media (Brief Tutorial/Review):

The governing equation for acoustic pressure in a porous material simplifies to the form of the familiar wave equation by defining an effective complex density and sound speed. These are defined as:

$$\rho_e = \rho_p \left[1 - i \frac{\Phi}{\rho_p \omega} \right] \tag{1}$$

and

$$c_e = c_p \left[1 - i \frac{\Phi}{\rho_p \omega} \right]^{-1/2} . \tag{2}$$

Where Φ is the flow resistance (i.e. the pressure drop per unit length of material per unit mean flow velocity averaged over the total cross-sectional area of the porous material), ρ_p is the effective gas density of the porous material, and c_p is the gas phase speed in the porous material [Ref. 2]. The wavenumber is:

$$k = \frac{\omega}{c_e} = \frac{\omega}{c_p}\left[1 - i\frac{\Phi}{\rho_p \omega}\right]^{1/2} \quad . \tag{3}$$

The governing equation for pressure in the porous media can then be written as:

$$\nabla^2 p + \left(\frac{\omega}{c_e}\right)^2 p = 0 \, . \tag{4}$$

In terms of the effective variables, the momentum equation is given by:

$$i\omega\rho_e \vec{q} = -\vec{\nabla} p \, . \tag{5}$$

At normal incidence, the impedance, i.e. the ratio of complex pressure to complex velocity, at the surface of the porous material is

$$\text{at } \theta_i = 0, \quad z_n = \frac{p(z=0)}{w(z=0)} = -i\rho_e c_e \cot\frac{\omega H}{c_e} \tag{6}$$

where θ_i is the incidence angle from the normal to the surface, H is the thickness of the porous layer of material, and w is the particle velocity in the direction of the normal, as shown in Figure 1.

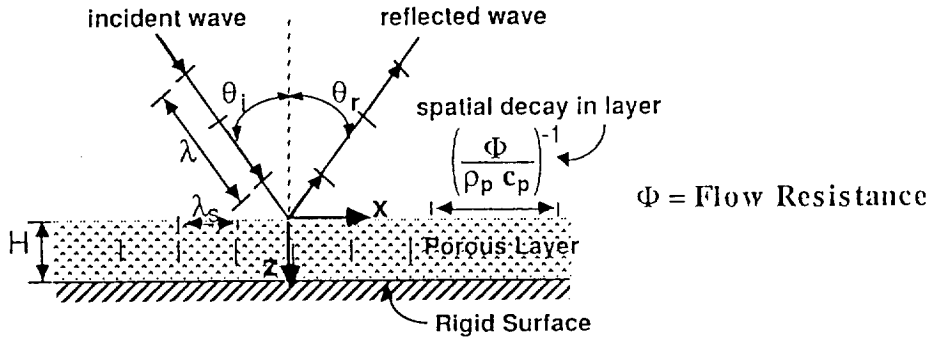

Figure 1. Sketch of porous material.

Boundary Condition Theoretical Development

For incidence angles other than normal incidence, the impedance is z_p, where z_p is defined below:

$$\text{For } \theta_i \neq 0, \quad z_p = \frac{p(z=0)}{w(z=0)} = -i\rho_e \frac{\omega}{k_z} \cot k_z H \tag{7}$$

The wavenumber component k_z is found from the dispersion relation:

$$-k_x^2 - k_z^2 + \frac{\omega^2}{c_e^2} = 0 \tag{8}$$

Re-writing the general incidence angle impedance equation, and multiplying and dividing the right-hand-side by $\cot[\omega H / c_e]$ yields:

$$p\left(1-\frac{k_x^{\,2}c_e^{\,2}}{\omega^2}\right)=-i\rho_e c_e\cot\left[\frac{\omega H}{c_e}\right]\frac{k_z H\cot[k_z H]}{\left(\frac{\omega H}{c_e}\right)\cot\left[\frac{\omega H}{c_e}\right]}w \tag{9}$$

Note that the ratio, $\frac{k_z H\cot[k_z H]}{\left(\frac{\omega H}{c_e}\right)\cot\left[\frac{\omega H}{c_e}\right]}=1$ when $k_x=0$ (i.e. normal impedance), and is *approximately equal* to 1 for low frequencies or high flow resistances (Φ). From geometry, the wavenumber component in the liner, k_z is given by:

$$k_z=(\omega/c_e)\left[1-(c/c_e)^2\sin^2\theta_i\right]^{1/2} \tag{10}$$

Liner of Infinite Thickness

Consider a porous layer of infinite thickness, such that $H\to\infty$, the impedance in this case becomes:

$$\frac{p(z=0)}{w(z=0)}=\frac{z_n}{\sqrt{1-(c/c_e)^2\sin^2\theta_i}} \tag{11}$$

For large flow resistance (Φ), the ratio $\frac{\Phi}{\rho_p\omega}>>1$ then,

$$\frac{p(z=0)}{w(z=0)}=z_n\left[1+\frac{i}{2}(c_p/c)^2\sin^2\theta_i\left(\frac{\Phi}{\rho_p\omega}\right)^{-1}\right] \tag{12}$$

Defining the pressure at the surface, p_s, and the particle velocity at the surface, w_s as $p_s=p(z=0)$ and $w_s=w(z=0)$, an approximate equation for p_s can be written as:

$$p_s+\left(\frac{i\rho_p c_p^{\,2}}{2\Phi\omega}\right)\left(\frac{-\omega^2\sin^2\theta_i}{c^2}\right)p_s=z_n w_s. \tag{13}$$

The quantity, $\left(\frac{-\omega^2\sin^2\theta_i}{c^2}\right)=k_s$ is the acoustic wavenumber component along the surface. This result can be re-expressed in terms of spatial variables. Defining the surface Laplacian operator as:

$$\nabla_s^{\,2}=\left.\frac{\partial^2}{\partial^2 x}+\frac{\partial^2}{\partial^2 y}\right|_{z=0} \tag{14}$$

Equation 13 can be rewritten in terms of the surface Laplacian:

$$p_s+\left(\frac{i\rho_p c_p^{\,2}}{2\Phi\omega}\right)\nabla_s^{\,2}p_s=z_n w_s \tag{15}$$

or in general:

$$p_s+B(\omega)\nabla_s^{\,2}p_s=z_n(\omega)w_s \tag{16}$$

Thin Layer

Now consider instead a thin layer, such that $\left|\frac{\omega H}{c_e}\right| << 1$. The normal impedance is approximately: $z_n \cong -i\rho_e c_e^{\,2}/\omega H$. For a thin layer the acoustic wavelength is assumed to be much greater than the thickness of the porous layer (H). In this limit, an equation for the surface pressure becomes:

$$p_s + \left(\frac{c_e^{\,2}}{\omega^3}\right)\left(\frac{-\omega^2 \sin^2\theta_i}{c^2}\right)p_s = z_n w_s \tag{17}$$

which is the "thin layer" version of Equation (13). Once again a general equation can be written in terms of the surface Laplacian:

$$p_s + B(\omega)\nabla_s^{\,2} p_s = z_n(\omega) w_s \tag{18}$$

Of course, the $B(\omega)$ are different functions in the two cases.

In Figures 2 through 4, sound absorption coefficients for different incidence angles are plotted versus nondimensional frequency. The sound absorption coefficients have been computed using the exact result (Eqn. 9), the thin layer result (Eqn. 17), and using the *normal incidence* impedance boundary condition instead of the bulk-reaction boundary condition. Results are shown for different angles of incidence, 45° (moderate incidence) and 80° (grazing incidence) and for different porous materials. Figure 2, corresponds to high flow resistance, Figure 3 is for a moderate flow resistance, and Figure 4 is for a low flow resistance. Notice, at high flow resistance there is little communication within the liner, resulting in only small errors from assuming normal incidence impedance. However, as the flow resistance decreases, the errors resulting from the normal incidence assumption increase to unacceptable values. Obviously this is due to increased communication within the liner (i.e., not a point-reacting material).

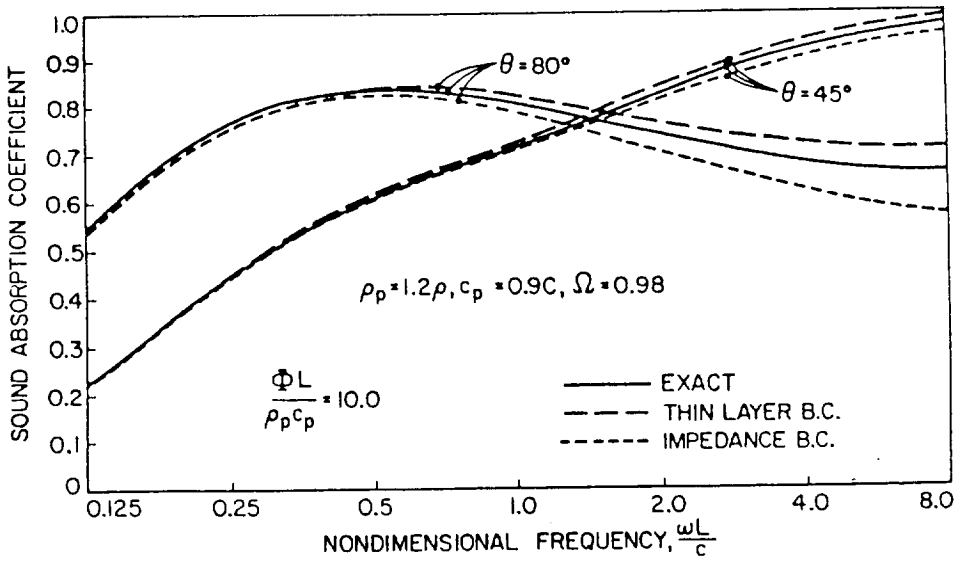

Figure 2. Comparison of absorption coefficients for different incidence angles, for a high flow resistance.

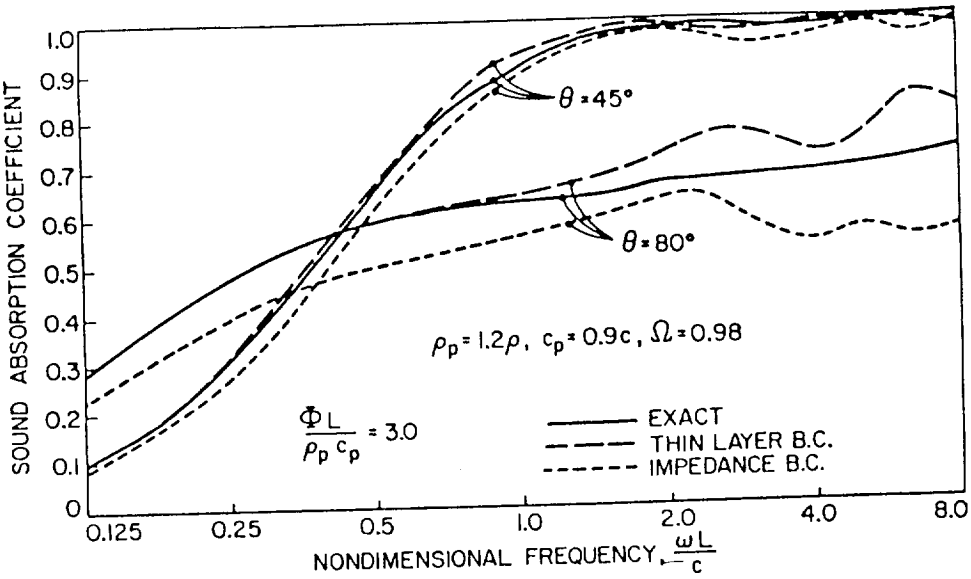

Figure 3. Comparison of absorption coefficients for different incidence angles, for a moderate flow resistance.

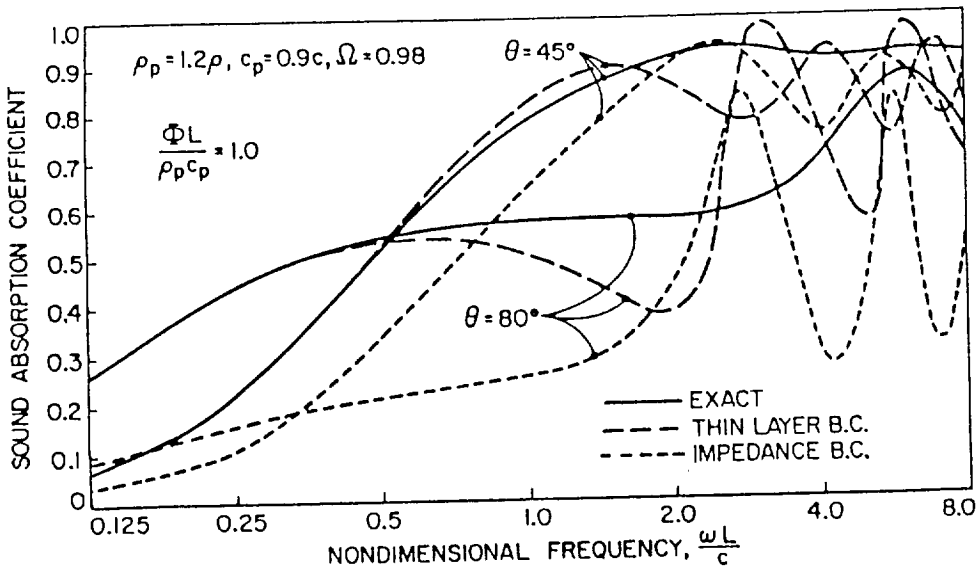

Figure 4. Comparison of absorption coefficients for different incidence angles, for a low flow resistance.

Extension to Higher Frequency

The general form of the impedance equation (i.e. relating pressure and velocity at the surface) can be extended to higher frequency. Equation (9) is rewritten here for reference:

$$p\left(1-\frac{k_x^{\,2}c_e^{\,2}}{\omega^2}\right)=-i\rho_e c_e \cot\left[\frac{\omega H}{c_e}\right]\frac{k_z H\cot[k_z H]}{\left(\frac{\omega H}{c_e}\right)\cot\left[\frac{\omega H}{c_e}\right]}w. \qquad (9)$$

In previous discussions, the ratio, $\dfrac{k_z H\cot[k_z H]}{\left(\frac{\omega H}{c_e}\right)\cot\left[\frac{\omega H}{c_e}\right]}$ was assumed approximately equal to unity. To extend the boundary condition results to higher frequency, Equation (9) is rewritten as a ratio of pressure to velocity. Substituting for k_zH as defined in Equation (10), and expanding the right-hand-side as a Taylor Series in powers of (c_e/c), leads to the following approximation:

$$\frac{p(z=0)}{w(z=0)}\cong z_n\left[1-\frac{1}{2}(c_e/c)^2\sin^2\theta_i+\frac{1}{8}(c_e/c)^4\sin^4\theta+\ldots\right]^{-1} \qquad (19)$$

In general, this can be written as:

$$\frac{p(z=0)}{w(z=0)}\cong z_n\left[1+B_2(\omega)k_x^{\,2}+B_4(\omega)k_x^{\,4}+\ldots\right]^{-1} \qquad (20)$$

Expressing this result using the surface Laplacian:

$$p_s+\tilde{B}_2(\omega)\nabla_s^{\,2}p_s+\tilde{B}_4(\omega)\nabla_s^{\,4}p_s=z_n(\omega)w_s \qquad (21)$$

In Figures 5 through 8 results are shown comparing the "impedance" (i.e., the ratio of p_s to w_s) for the different levels of approximation. Figures 5 and 6 show the real part and the imaginary part, respectively, over the entire dimensionless frequency range. In Figures 7 and 8, the scale has been expanded to emphasize the low frequency range.

An absorption coefficient based on these impedance values can be obtained. In Figures 9 and 10, the corresponding absorption coefficients are shown for the different boundary condition assumptions. In all cases, assuming normal incidence impedance results in erroneous results. Assuming a bulk-reacting boundary condition shows improvement, although it appears that there is little difference between retaining the B_4 term and only retaining the B_2 term.

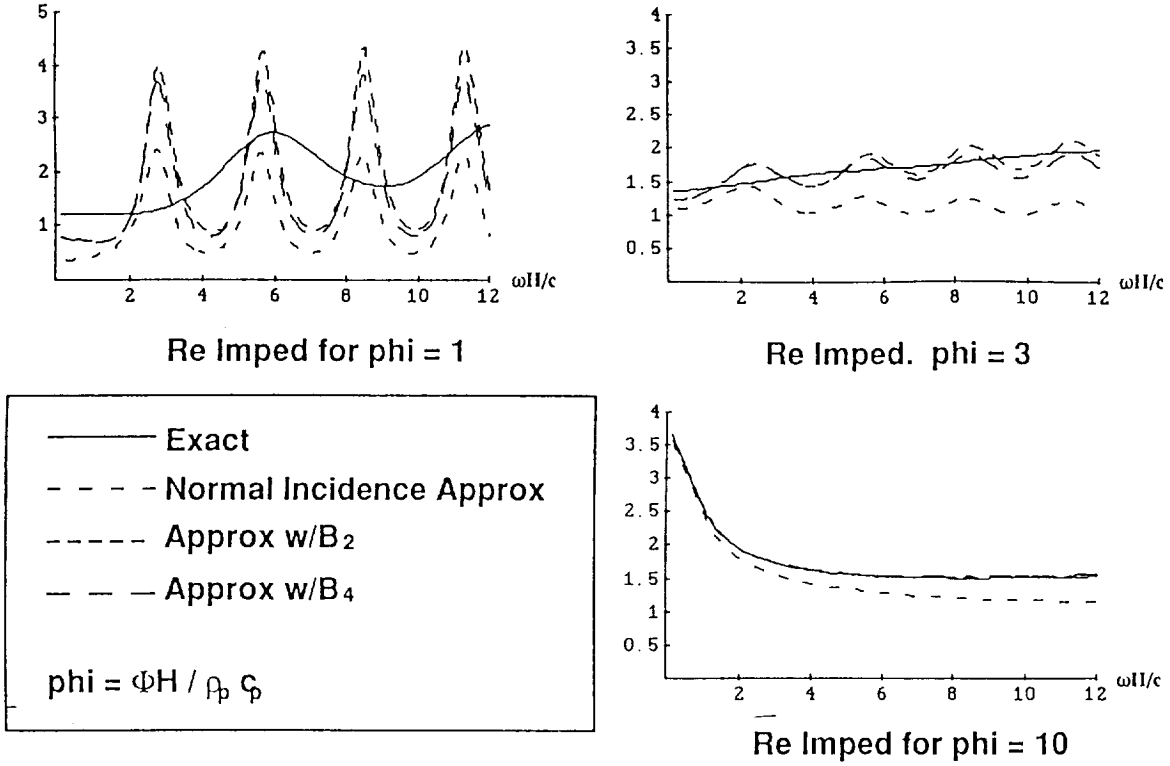

Figure 5. Real part of the impedance (p_s/w_s) versus dimensionless frequency for different flow resistance parameters. Comparison between different levels of boundary condition approximation.

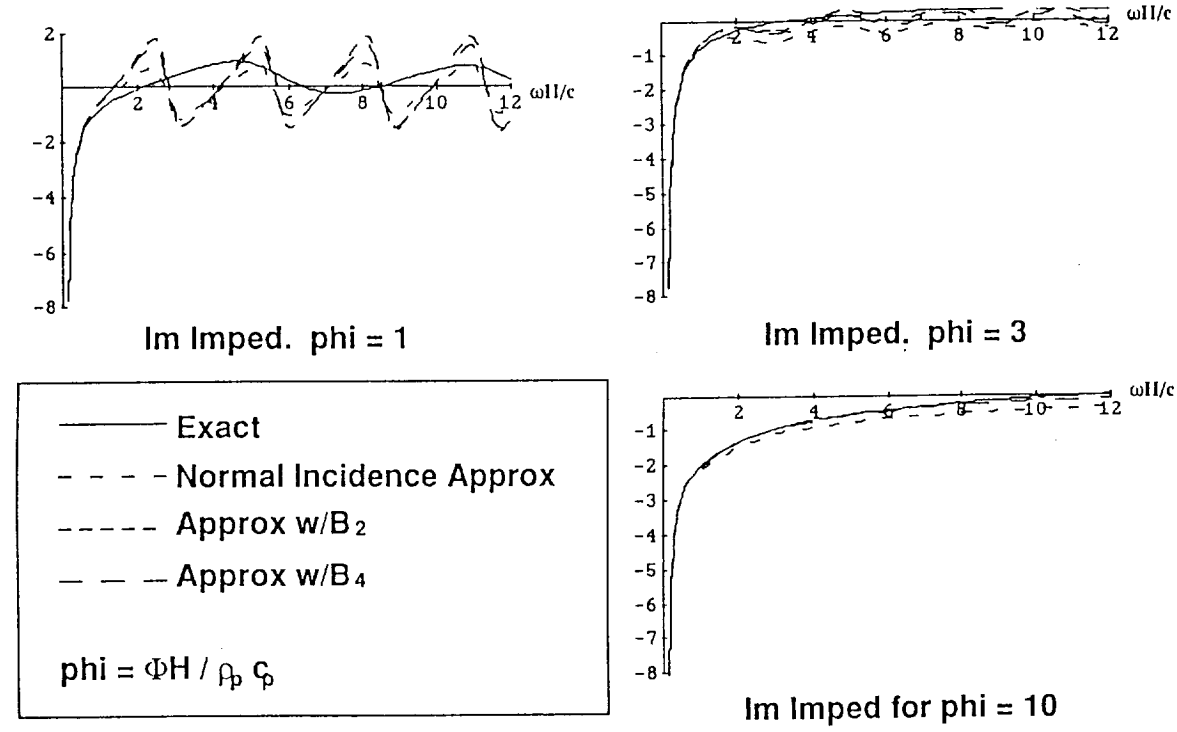

Figure 6. Imaginary part of the impedance versus dimensionless frequency for different flow resistance parameters. Comparison between different levels of boundary condition approximation.

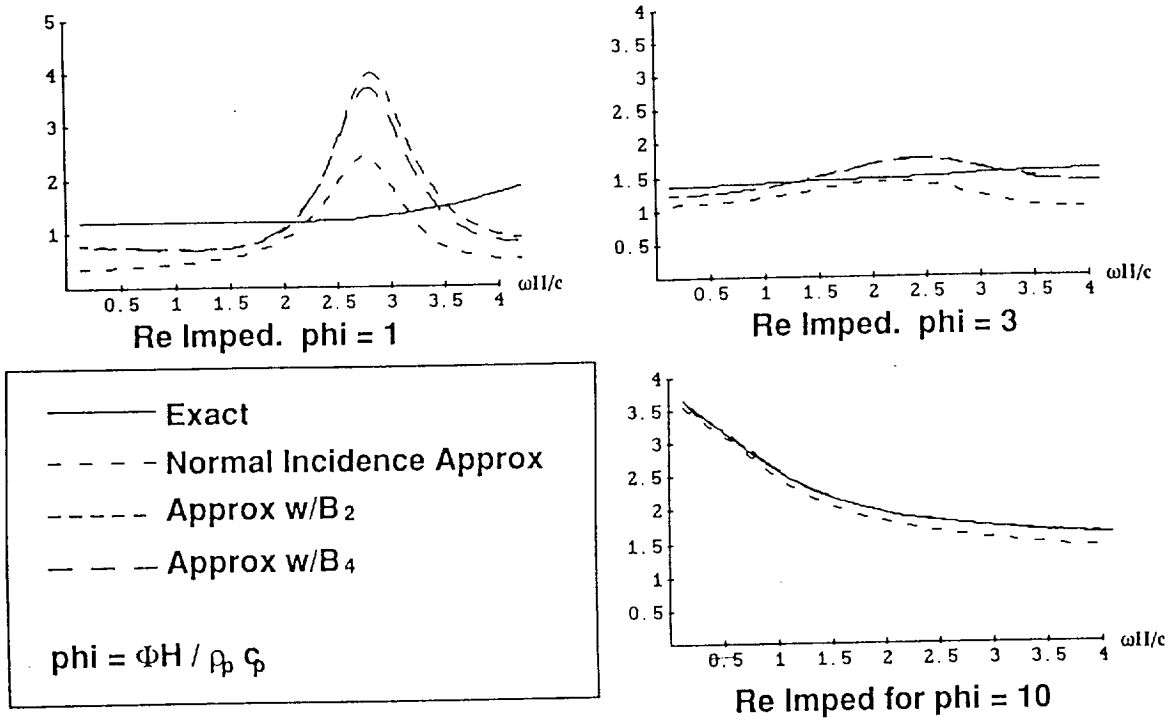

Figure 7. Real part of the impedance (p_s/w_s) versus dimensionless frequency for different flow resistance parameters. Comparison between different levels of boundary condition approximation.

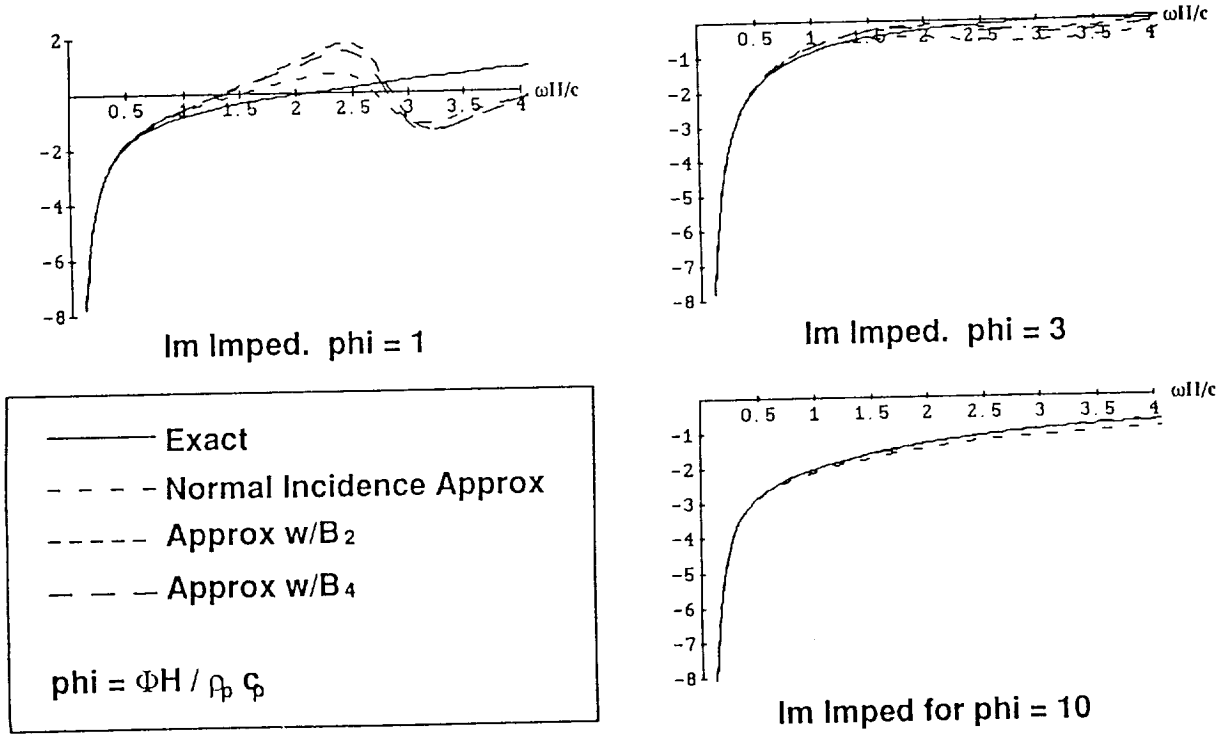

Figure 8. Imaginary part of the impedance versus dimensionless frequency for different flow resistance parameters. Comparison between different levels of boundary condition approximation.

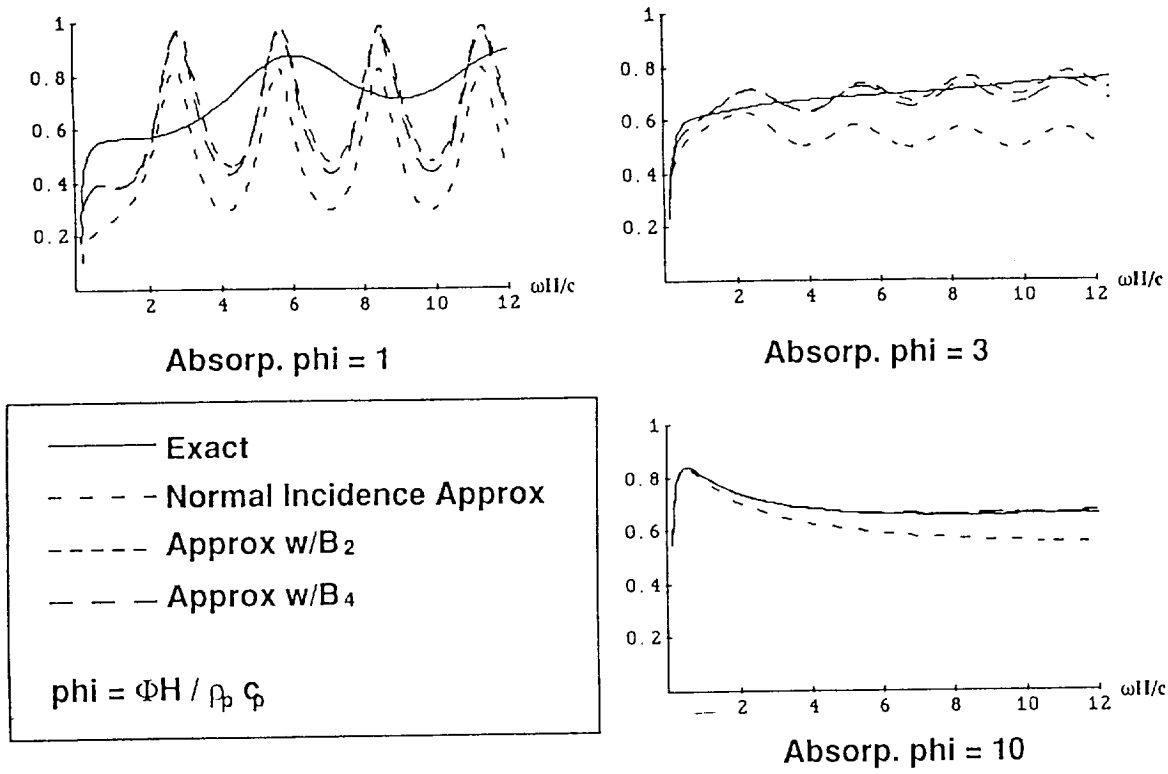

Figure 9. Absorption coefficients versus dimensionless frequency over the entire frequency range. Comparison between different levels of boundary condition approximation.

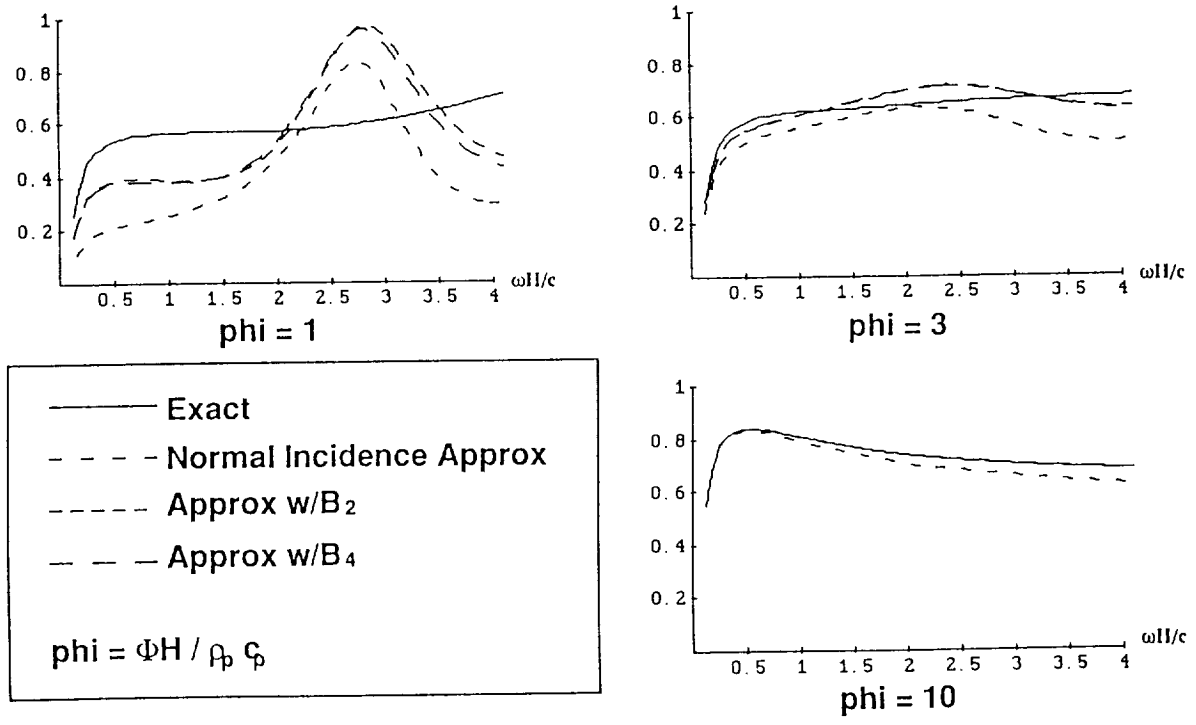

Figure 10. Absorption coefficients versus dimensionless frequency over the low frequency range. Comparison between different levels of boundary condition approximation.

Experimental Determination of Coefficients

The coefficients, B_2 and B_4 can be determined experimentally in a bulk reaction duct, by measuring characteristics of the standing wave patterns. This idea is similar to that of determining normal incidence impedance values from standing wave patterns in an impedance tube. However, the bulk reaction duct is a different device, and the porous material is mounted along the sides of the duct. See Figure 11, for a sketch of a bulk reaction duct. An example of determining the coefficient B_2 from a bulk reaction duct is explained in Reference [3].

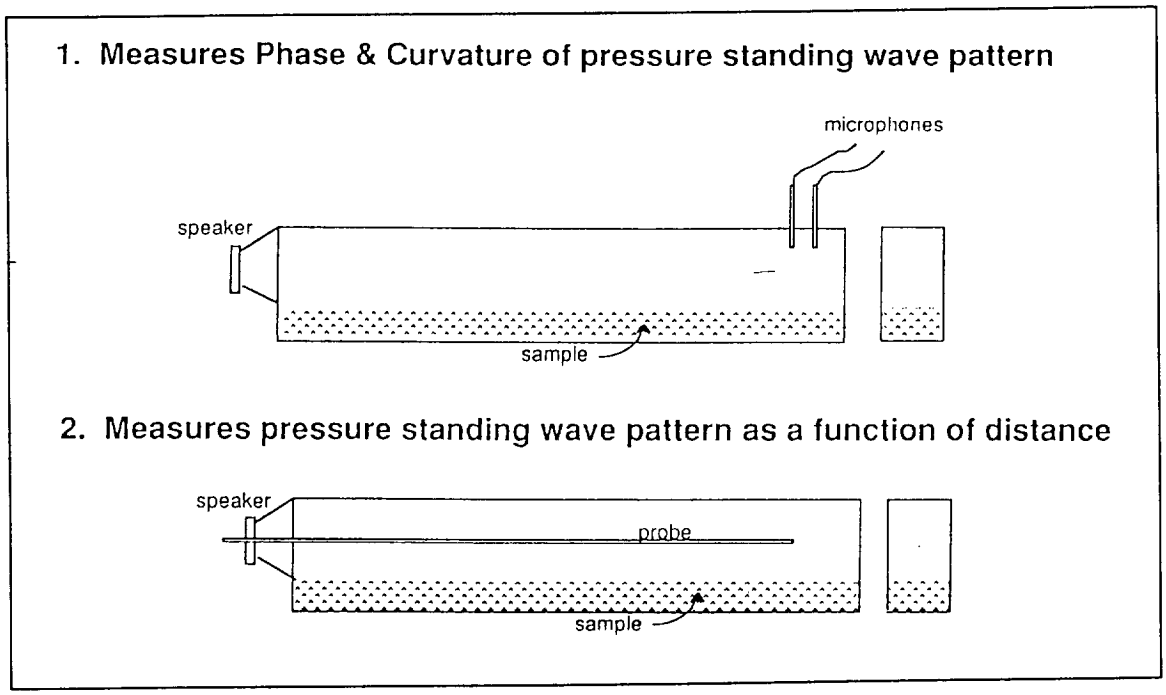

Figure 11. Sketch of a bulk reaction duct (2 possibilities).

For a duct of height h, solution of the wave equation in the duct and application of the momentum equation result in an expression for the surface impedance:

$$\frac{p(z=0)}{w(z=0)} = i\rho_o c \frac{k}{k_z} \cot(k_z h) \tag{22}$$

However, the surface impedance from the above boundary condition derivation is:

$$\frac{p(z=0)}{w(z=0)} = \frac{\rho_o c z_n(\omega)}{\left(1 + B_2(\omega) k_x{}^2 + B_4(\omega) k_x 4\right)} \tag{22}$$

in terms of the Bulk Reaction Coefficients, B_2 and B_4. As explained in Reference [3] the coefficients are determined from standing wave patterns. Example standing wave patterns are shown in Figure 12 for porous materials with different flow resistances.

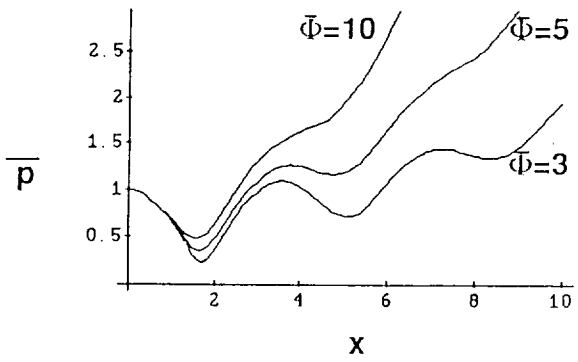

Figure 12. Sample standing wave patterns from materials with different flow resistances.

Time Domain Boundary Condition

A very important issue was the development of the corresponding boundary conditions for use in a time domain analysis, since a time domain approach may be used to analyze the acoustic field within the nacelle. The approach taken was to express the time domain boundary condition in terms of an impulse response function. The impulse response function used generated the surface velocity time history for an impulsive input in surface pressure (and more generally, in terms of step inputs in spatial derivatives of pressure). The liner response to an arbitrary pressure field could then be constructed in terms of a superposition integral. In such a formulation, the surface normal velocity would depend on an integral of the time rate of change of the surface pressure and its derivatives weighted with the time delayed impulse response function.

This approach was similar to using a convolution or a superposition integral. The impulse response function itself forms a Fourier transform pair with a quantity involving the frequency domain boundary response function, essentially the boundary condition of the general form described by Equation (21). The derivation of a time domain boundary condition follows:

Convert from frequency to time domain by Fourier Transforms

$$f(\omega)=\int_{-\infty}^{+\infty} f(t)e^{-i\omega t}dt \quad \text{and} \quad f(t)=\frac{1}{2\pi}\int_{-\infty}^{+\infty} f(\omega)e^{+i\omega t}d\omega \tag{22}$$

In the frequency domain, the boundary condition can be written as:

$$w_s(x,y,\omega)=\frac{1}{z_n}p_s(x,y,\omega)+\frac{B_2(\omega)}{z_n(\omega)}\nabla_s{}^2 p_s(x,y,\omega)+\frac{B_4(\omega)}{z_n(\omega)}\nabla_s{}^4 p_s(x,y,\omega) \tag{23}$$

Applying the inverse transform to Equation (23):

$$w_s(x,y,t)=\frac{1}{2\pi}\int_{-\infty}^{+\infty}\frac{1}{z_n}p_s(x,y,\omega)e^{i\omega t}d\omega+\frac{1}{2\pi}\int_{-\infty}^{+\infty}\frac{B_2(\omega)}{z_n(\omega)}\nabla_s{}^2 p_s(x,y,\omega)e^{i\omega t}d\omega+\frac{1}{2\pi}\int_{-\infty}^{+\infty}\frac{B_4(\omega)}{z_n(\omega)}\nabla_s{}^4 p_s(x,y,\omega)e^{i\omega t}d\omega \tag{24}$$

Similarly, the surface Laplacian operators operating on the surface pressure can be transformed:

$$\nabla_s{}^4\ p_s(x,y,\omega)=\int_{-\infty}^{+\infty}\nabla_s{}^4\ p_s(x,y,t)e^{-i\omega t}dt \tag{25}$$

$$\nabla_s{}^2\ p_s(x,y,\omega)=\int_{-\infty}^{+\infty}\nabla_s{}^2\ p_s(x,y,t)e^{-i\omega t}dt \tag{26}$$

The Fourier transform of the time-dependent pressure is:

$$p_s(x,y,\omega)=\int_{-\infty}^{+\infty}p_s(x,y,t)e^{-i\omega t}dt \tag{27}$$

Using Equations (25) through (27) in Equation (24) yields:

$$w_s(x,y,t)=\int_{-\infty}^{+\infty}p_s(x,y,\tau)\left[\frac{1}{2\pi}\int_{-\infty}^{+\infty}\frac{1}{z_n}e^{i\omega(t-\tau)}d\omega\right]d\tau+\int_{-\infty}^{+\infty}\nabla_s{}^2 p_s(x,y,\omega)\left[\frac{1}{2\pi}\int_{-\infty}^{+\infty}\frac{B_2(\omega)}{z_n(\omega)}e^{i\omega(t-\tau)}d\omega\right]d\tau+\int_{-\infty}^{+\infty}\nabla_s{}^4 p_s(x,y,\omega)\left[\frac{1}{2\pi}\int_{-\infty}^{+\infty}\frac{B_4(\omega)}{z_n(\omega)}e^{i\omega(t-\tau)}d\omega\right]d\tau \tag{28}$$

where the Impulse Response Functions are given by the terms in square brackets.

Defining the Impulse Response Functions as, I_0, I_2, I_4:

$$I_o(s)=\frac{1}{2\pi}\int_{-\infty}^{+\infty}\frac{1}{z_n}e^{i\omega s}d\omega \tag{29}$$

$$I_2(s)=\frac{1}{2\pi}\int_{-\infty}^{+\infty}\frac{B_2(\omega)}{z_n(\omega)}e^{i\omega s}d\omega \tag{30}$$

$$I_4(s)=\frac{1}{2\pi}\int_{-\infty}^{+\infty}\frac{B_4(\omega)}{z_n(\omega)}e^{i\omega s}d\omega \tag{31}$$

Equation (28) can be re-written in terms of the Impulse Response Functions:

$$w_s(x,y,t)=\int_{-\infty}^{+\infty}p_s(x,y,\tau)I_o(t-\tau)d\tau+\int_{-\infty}^{+\infty}\nabla_s{}^2 p_s(x,y,\omega)I_2(t-\tau)d\tau+\int_{-\infty}^{+\infty}\nabla_s{}^4 p_s(x,y,\omega)I_4(t-\tau)d\tau \tag{32}$$

where, $s\equiv(t-\tau)$.

The impulsive pressure at the surface is given by (as shown in Figure 13):

$$p_s(x,y,t)=P(x,y)\delta(t-\tau) \tag{33}$$

The integrals in Equation (32) can be evaluated using contour integration (see Figure 14).

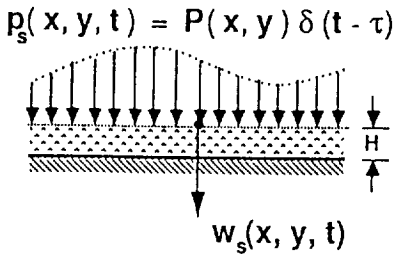

Figure 13. Sketch of impulsive pressure applied to surface of liner of thickness H.

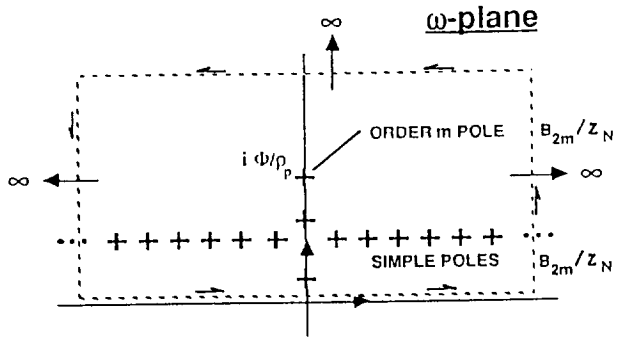

Figure 14. Schematic of the contour integration.

The first two integrals corresponding to the impulse response functions evaluate to:

$$I_o(s) = \frac{c_p/H}{\rho_p c_p}\sum_{n=1}^{\infty}\left[(-1)^{n+1}2\delta(s-2n) + 2\cos(w_n\hat{s}) - 2\cos\left(\frac{(2n-1)\pi}{2}\hat{s}\right) - \overline{\Phi}\frac{\sin(w_n\hat{s})}{w_n}\right]e^{-\frac{\overline{\Phi}}{2}\hat{s}}$$

$$I_2(s) = \frac{(c_p/H)H^2}{\rho_p c_p}\left[-\frac{1}{2}e^{-\overline{\Phi}\hat{s}} + \frac{2}{\pi^2}\sum_{n=1}^{\infty}\left[\frac{2\cos(w_n\hat{s})}{(2n-1)^2} - \overline{\Phi}\frac{\sin(w_n\hat{s})}{(2n-1)^2 w_n}\right]e^{-\frac{\overline{\Phi}}{2}\hat{s}}\right]$$

where $w_n = \sqrt{(2n-1)^2(\pi/2)^2 - (\overline{\Phi}/2)^2}$, $\overline{\Phi} = \dfrac{\Phi H}{\rho_p c_p}$, and $\hat{s} = \dfrac{c_p}{H}s$

Figures 15 and 16 show plots of the impulse response functions I_o and I_2 for different flow resistances. Note that the delta functions correspond to reflections of the impulse. The impulse response functions exhibit a relaxation and reflection structure. After the impulse, there is a velocity relaxation (temporal wake) that results from the flow resistance. The relaxation time scales with ρ_p/Φ. If the damping is not too great, wave reflections (discontinuities) are evident. The reflection time scale corresponds to: H/c_p. In Figure 15, I_o is shown. For Io(s) the delta function amplitudes scale with $1/\rho_p c_p$. For Io(s), the relaxation structure scales with $\Phi H/\rho_p c_p$, and increases with increasing $\Phi H/\rho_p c_p$.

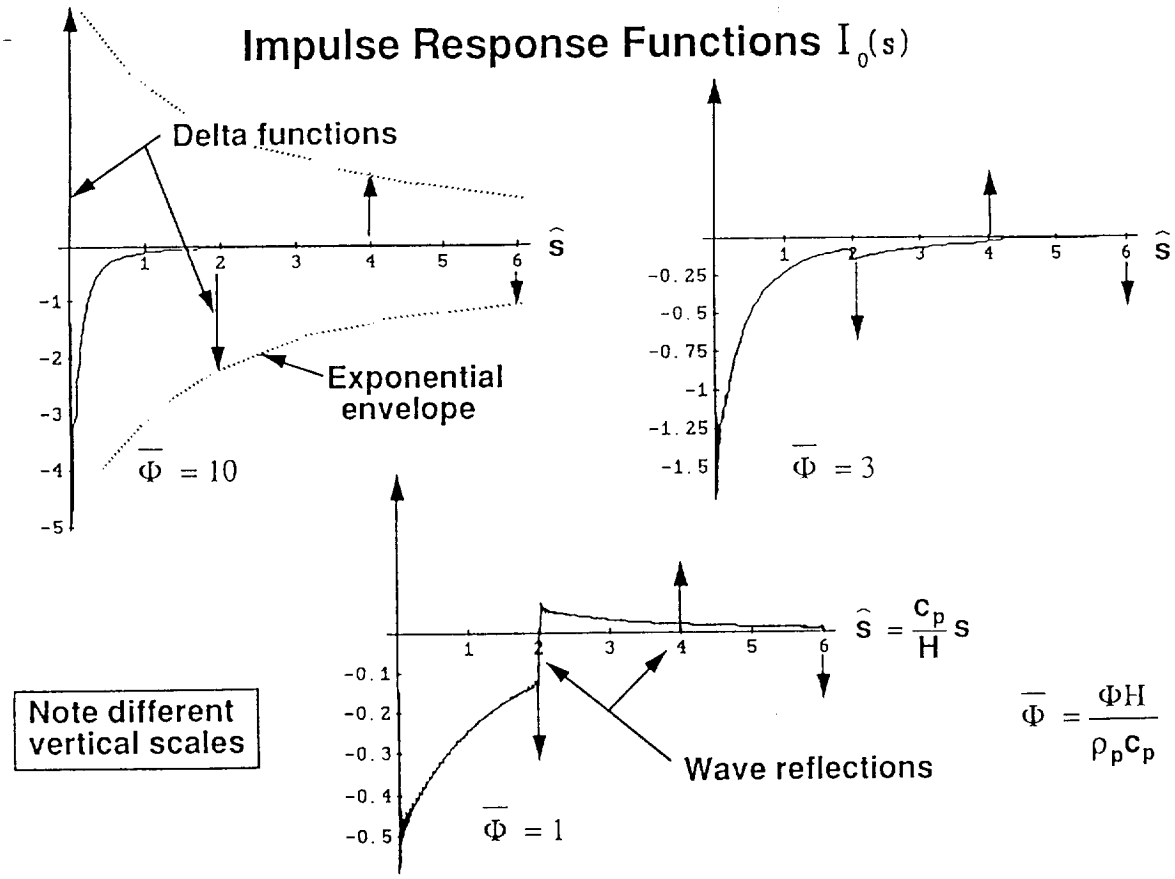

Figure 15. Plots of impulse response function, I_o versus dimensionless time.

In Figure 16, I_2 is shown. For $I_2(s)$ and $I_4(s)$ the relaxation structure decreases with increasing $\Phi H/\rho_p c_p$. The lower flow resistance facilitates bulk reaction. The reflection structure is always stronger for lower $\Phi H/\rho_p c_p$, since reflections decay as $e^{-\frac{1}{2}(\Phi/\rho_p)\hat{s}}$.

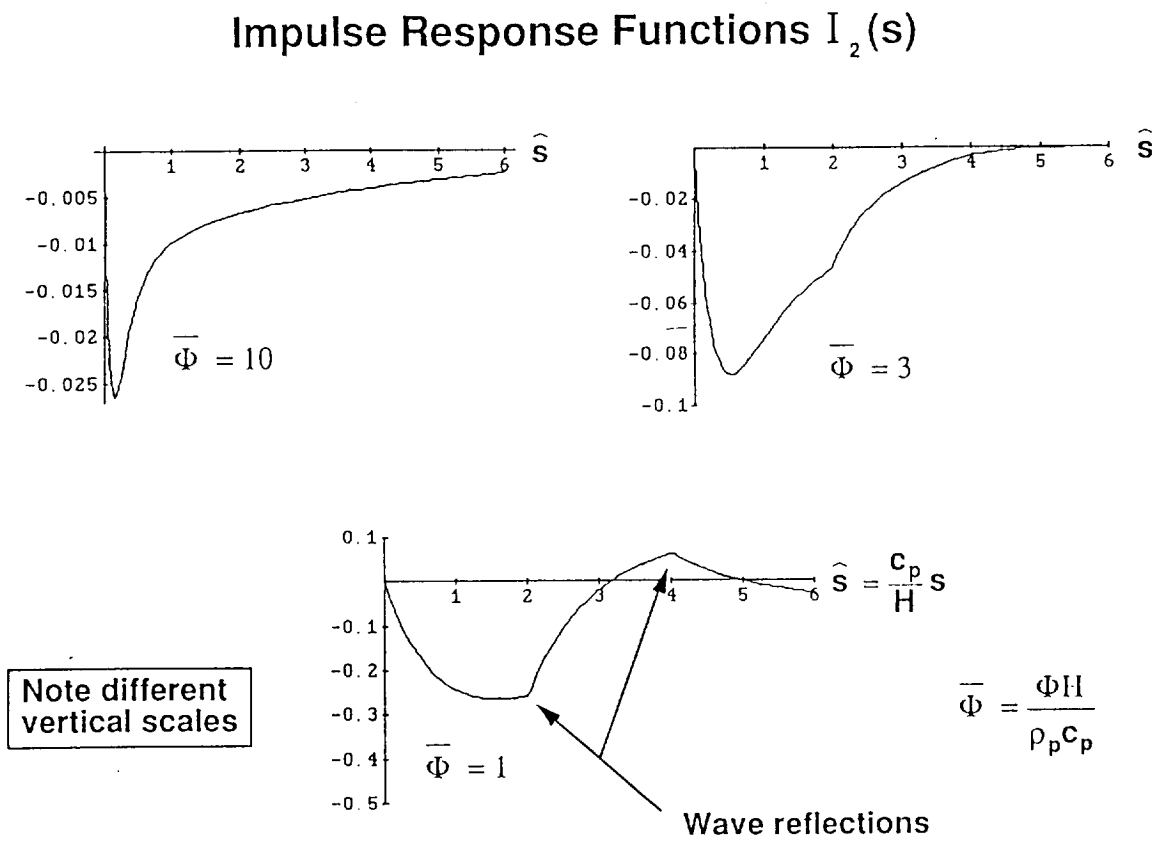

Figure 16. Plots of impulse response function, I_2 versus dimensionless time.

Numerical Implementation

Implementation of the boundary condition in a time-domain numerical calculation scheme for duct acoustics would require saving information about pressure and pressure derivatives on the liner surface from previous time steps. However, since it was assumed that effective liner designs would embody high absorption, it was thought likely that the liner dynamics would be highly damped. This would limit the amount of information that would have to have been retained from previous time steps in order to evaluate the superposition integral.

Summary & Conclusions

Earlier results were extended to higher frequency. This was done by first working up from the low frequency end, adding higher order corrections. These corrections were found to extend the boundary condition to somewhat higher frequencies (into the mid frequency range). The final result combined aspects of both the high and low frequency approximations, and yielded good accuracy across the entire frequency range for realistic values of porous media parameters (flow resistance, etc.). The form of the boundary condition was similar to earlier work, but the coefficients were chosen differently. Expressions for the bulk reaction coefficients were found for a layer of rigid homogeneous porous material.

The restriction on the boundary condition which has been developed is that the liner have a fairly high flow resistance, which is typical of realistic porous liners. The high flow resistance limits the degree of communication between points along the liner surface by damping the waves within the liner. For the boundary condition to work well, the dissipation length scale must be on the order of the liner thickness at high frequency, which is a realistic condition. Comparisons of absorption coefficient have shown excellent agreement for different levels of approximation, and different incidence angles.

The boundary condition approach retains considerable simplicity in comparison to a full solution for wave motion within a liner. Furthermore, the coefficients in this boundary condition can be measured experimentally, as well as calculated theoretically. Therefore the boundary condition retains a significant advantage of the traditional impedance approach. Although the approach was developed for a simple porous media layer, the method can be generalized to a much broader class of liner configurations. In fact, the approach is general in much the same way that the impedance concept itself is general, namely that the same representation can be applied to a broad variety of materials and dynamic systems.

An important aspect is the possibility that the frequency dependent coefficients $B_2(\omega)$, and $B_4(\omega)$ can be determined experimentally. It may be difficult, or inconvenient, to predict liner behavior from basic material properties, especially for complicated multi-layer liner designs. In fact the necessary material properties may not be well known and may themselves require measurement. A more realistic approach may be to measure the boundary condition coefficients directly. The normal incidence impedance $z_n(\omega)$ can be measured by traditional means using an impedance tube. Reference [3] showed how, in general, bulk reaction coefficients can be measured at low frequency using a "bulk reaction duct," a device invented for that purpose. The bulk reaction duct is similar in general concept to an impedance tube, but the absorptive liner is placed on a side wall of the rectangular duct. Properties of the sound field are measured to infer the bulk reaction coefficients given the normal impedance and the functional form of the boundary condition.

A time domain version of the boundary condition was constructed from inverse Fourier transforms and impulse response functions. The frequency dependent coefficients in the frequency domain boundary condition $z_n(\omega)$,$B_2(\omega)$, and $B_4(\omega)$ for the simple porous layer can be fit by functional forms that facilitate transform inversion. The time domain version can be implemented in a straight-forward manner into a numerical code.

References

1. "State of the Art in Duct Acoustics," P.G. Vaidya and P. D. Dean, AIAA paper No. 77-1279, presented at the AIAA 4th Aeroacoustics Conference (1977).

2. "A Study of Bulk Reacting Porous Sund Absorbers and a New Boundary Condition for Thin Porous Layers," D. B. Bliss, J. Acoust. Soc. Am. 71(3), 1982.

3. "Experimental Investigation of the Bulk Reaction Boundary Condition," D. B. Bliss and S. E. Burke, J. Acoust. Soc. Am., 71(30), 1982.